

Probing microscopic models for system-bath interactions via parametric driving

Anastasia S. D. Dietrich¹, Martin Kiffner^{2,1}, and Dieter Jaksch^{1,2}

*Clarendon Laboratory, University of Oxford, Parks Road, Oxford OX1 3PU, United Kingdom¹ and
Centre for Quantum Technologies, National University of Singapore, 3 Science Drive 2, Singapore 117543²*

(Dated: March 22, 2018)

We show that strong parametric driving of a quantum harmonic oscillator coupled to a thermal bath allows one to distinguish between different microscopic models for the oscillator-bath coupling. We consider a bath with an Ohmic spectral density and a model where the system-bath interaction can be tuned continuously between position and momentum coupling via the coupling angle α . We derive a master equation for the reduced density operator of the oscillator in Born-Markov approximation and investigate its quasi-steady state as a function of the driving parameters, the temperature of the bath and the coupling angle α . We find that the time-averaged variance of position and momentum exhibits a strong dependence on these parameters. In particular, we identify parameter regimes that maximise the α -dependence and provide an intuitive explanation of our results.

I. INTRODUCTION

Accurate models for the interaction between a quantum system and its environment have been vital for the success of quantum optics and cold atom systems. For example, they have paved the way for revolutionising methods such as laser cooling [1], and are essential for developing applications in quantum technologies where decoherence effects need to be as small as possible. For some systems our understanding of the system-bath coupling is so accurate that it can be used to control and engineer these interactions. In this way, the role of dissipation and decoherence can be transformed from a detrimental effect into a wanted feature as shown, e.g., in [2–8].

This is in stark contrast to condensed matter systems where the exact microscopic model underlying the system-bath coupling is often unknown [9], and thus one has to resort to phenomenological models. Driving these systems with intense terahertz radiation opens up unprecedented possibilities to manipulate their quantum dynamics [10–23]. Examples include the melting of charge density waves [10–12], the generation of synthetic magnetic fields [13], the control of heterointerfaces [14–16], the possibility to drive metal-insulator transitions [17, 18], the parametric cooling of bilayer cuprate superconductors [19], the control of transport modes in cuprate superconductors [20], or even the controlled creation of transient superconductivity [21–23]. In order to optimize the coherent control of these systems even further, it would be highly desirable to improve our understanding of their system-bath interactions.

A direct manifestation of system-bath interactions are decay and decoherence rates that can be directly observed in an experiment. However, these quantities reveal little about the microscopic details of the system-bath interaction, and additional steps need to be taken to uncover more details. For example, some information about the local spectral density of a condensed matter heat bath can be obtained by observing the non-Markovian behaviour of an opto-mechanical resonator coupled to it [24]. Alternatively, information about the system-

bath coupling can in principle be obtained by driving the system of interest so strongly that the driving modifies the system-bath interaction. This strongly-driven regime can be described within the framework of the Floquet-Markov master equation approach [25–30], which combines ideas from open quantum systems with Floquet theory [31–33]. For example, it has been shown [34] that the response of a strongly driven two-level system depends on the specific form of the coupling operator.

Here we consider a paradigmatic example for system-bath interactions comprised of a parametrically driven oscillator that is weakly coupled to a thermal bath, see Fig. 1. We show that the driving allows one to distinguish between microscopic models for the system-bath interaction H_I^α that can be tuned continuously from position to momentum coupling via the parameter α . We derive a master equation for the reduced density operator of the oscillator in Born-Markov approximation and find that its quasi-steady state exhibits a strong dependence on α due to the parametric driving. In particular, we consider the time-averaged variance of position and momentum and identify parameter regimes that maximise their α -dependence. We find that this α -dependence can be understood in terms of an effective model with an α -dependent spectral density that is probed at different Floquet quasi-frequencies. This also shows that strong driving allows investigating other aspects of system-bath interactions that go beyond measuring the value of α .

The paper is organised as follows. In Sec. II we present our model and discuss the steps and approximations leading to a master equation applicable to a strongly driven system. The presentation of our results in Sec. III begins with a description of the observables that we use to characterise the quasi-steady state of the oscillator in Sec. III A. Our numerical results for the time-averaged mean values of the system quadratures as a function of the coupling angle, bath temperature and driving parameters are presented in Sec. III B. In Sec. IV, we introduce a unitary transformation of the total Hamiltonian in order to explain the α -dependence of our results. Finally, we conclude with a summary and an outlook for further

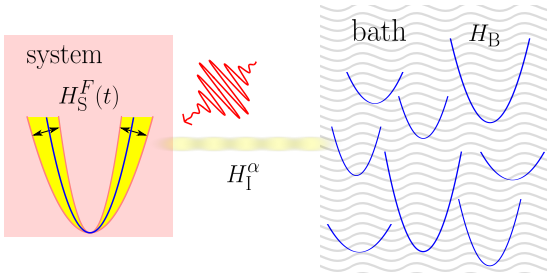


FIG. 1. (Color online) The system of interest is comprised of a parametrically driven harmonic oscillator and a bath of harmonic oscillators with Hamiltonians $H_S^F(t)$ and H_B , respectively. The system-bath interaction is described by the interaction Hamiltonian H_I^α , where the parameter α allows one to continuously adjust the interaction from position ($\alpha = 0$) to momentum coupling ($\alpha = \pi/2$). The parametric driving affects both the system and dissipation mechanism as indicated by the red arrow.

work in Sec. V.

II. MODEL

Here we describe our theoretical model for a driven harmonic oscillator coupled to a thermal bath. The isolated system is described in Sec. II A, and Sec. II B discusses the system-bath coupling.

A. Isolated system dynamics

We consider a harmonic oscillator with mass m and time-dependent frequency $\omega_F(t)$. The corresponding Hamiltonian is given by [35–41]

$$H_S^F(t) = \frac{p^2}{2m} + \frac{1}{2}m\omega_F^2(t)x^2, \quad (1)$$

where the position and momentum operators x and p obey the canonical commutation relation $[x, p] = i\hbar$. We assume that the oscillator frequency $\omega_F(t)$ is modulated periodically with frequency ω_L ,

$$\omega_F^2(t) = \omega_0^2[1 + F \cos(\omega_L t + \phi_L)], \quad (2)$$

where F is the relative modulation amplitude. Throughout this paper we assume that $F = 0$ for $t < 0$. It follows that the Hamiltonian in Eq. (1) reduces to an ordinary harmonic oscillator with frequency ω_0 and mass m for negative times. In our model the driving amplitude is suddenly switched on at $t = 0$ and held at a constant value for $t > 0$.

The time-dependent Schrödinger equation associated with the Hamiltonian in Eq. (1) can be solved exactly [41–45],

$$i\hbar \frac{\partial}{\partial t} \psi_n(x, t) = H_S^F(t) \psi_n(x, t). \quad (3)$$

The solutions $\psi_n(x, t)$ ($n = 0, 1, 2, \dots$) are described in Appendix A and reduce to the familiar harmonic oscillator states for $F = 0$. It is possible to introduce generalized creation and annihilation operators that operate on the states $\psi_n(x, t)$ like in the undriven harmonic oscillator [28],

$$A(t)|\psi_n(t)\rangle = \sqrt{n}|\psi_{n-1}(t)\rangle, \quad (4a)$$

$$A^\dagger(t)|\psi_n(t)\rangle = \sqrt{n+1}|\psi_{n+1}(t)\rangle. \quad (4b)$$

Note that the operators A and A^\dagger are time-dependent.

Time-dependent Hamiltonians do generally not guarantee the validity of uncertainty relations and commutation relations [43]. However, the solution to the isolated system dynamics for our system Hamiltonian in Eq. (1) does not violate the uncertainty and commutation relations between canonical position and momentum operators [45].

B. System-bath coupling

We assume that the driven oscillator is weakly coupled to a heat bath of N harmonic oscillators with Hamiltonian

$$H_B = \sum_{r=1}^N \left(\frac{p_r^2}{2m_r} + \frac{1}{2}m_r\omega_r^2 x_r^2 \right). \quad (5)$$

Here position and momentum operators of the r th oscillator with mass m_r and frequency ω_r are denoted by operators x_r and p_r , respectively. The coupling between the bath and system is described by the Hamiltonian

$$H_I^\alpha = -c_\alpha B, \quad (6)$$

where the parameter α in the coupling operator

$$c_\alpha = \cos(\alpha)x + \sin(\alpha)\frac{p}{m\omega_0} \quad (7)$$

describes which degrees of freedom are coupled to the bath. Note that $c_{\alpha=0}$ corresponds to position coupling, and $c_{\alpha=\pi/2}$ realises momentum coupling [46–49]. The bath operator B in Eq. (6) is given by

$$B = \sum_{r=1}^N \kappa_r x_r, \quad (8)$$

and κ_r are coupling constants. The system-bath interaction Hamiltonian in Eq. (6) thus couples the system operator c_α to the position operators of the bath.

With the definitions in Eqs. (1), (5) and (6) we arrive at the total Hamiltonian for the driven oscillator coupled to the bath,

$$H^\alpha = H_S^F(t) + H_B + H_I^\alpha. \quad (9)$$

We assume the coupling to the bath to be weak and describe the quantum dynamics of the reduced density operator of the system ρ by a Born-Markov master equation [26],

$$\dot{\rho} = -\frac{i}{\hbar} [H_S^F(t), \rho] + \mathcal{K}\rho, \quad (10)$$

where the first term describes the coherent evolution and $\mathcal{K}\rho$ accounts for the interaction with the heat bath at temperature T ,

$$\mathcal{K}\rho = -\frac{1}{\hbar^2} \int_0^\infty d\tau \text{Tr}_B \left\{ \left[H_I^\alpha, \left[\tilde{H}_I^\alpha(t-\tau, t), \rho_B \otimes \rho(t) \right] \right] \right\}. \quad (11)$$

Here

$$\rho_B = \exp\left(-\frac{H_B}{k_B T}\right) / \text{Tr}_B \left\{ \exp\left(-\frac{H_B}{k_B T}\right) \right\} \quad (12)$$

is the density operator of the bath in thermal equilibrium and k_B is Boltzmann's constant. The operator \tilde{H}_I^α in Eq. (11) is defined as

$$\tilde{H}_I^\alpha(t, t_0) = [U_S(t, t_0) U_B(t, t_0)]^\dagger H_I^\alpha [U_S(t, t_0) U_B(t, t_0)], \quad (13)$$

where $U_B(t, t_0) = \exp[-(i/\hbar)H_B(t-t_0)]$ describes the free evolution of the bath. The time evolution operator of the system is

$$U_S(t, t_0) = \begin{cases} \mathcal{T}_+ \exp\left(-\frac{i}{\hbar} \int_{t_0}^t dt' [H_S^F(t')]\right), & t \geq t_0, \\ \mathcal{T}_- \exp\left(\frac{i}{\hbar} \int_t^{t_0} dt' [H_S^F(t')]\right), & t < t_0, \end{cases} \quad (14)$$

where \mathcal{T}_+ and \mathcal{T}_- are the chronological and anti-chronological time ordering operators, respectively.

In order to evaluate Eq. (11) we later assume that the heat bath exhibits an Ohmic spectral density with a Lorentz-Drude cutoff $\Omega \gg \omega_0$ [26], i.e.

$$J(\omega) = \frac{1}{\pi} \gamma \omega m \frac{\Omega^2}{\Omega^2 + \omega^2}, \quad (15)$$

where γ is the decay rate. With these assumptions Eq. (11) can be written as (see Appendix B)

$$\mathcal{K}\rho = \frac{1}{\hbar} \int_{-\infty}^{\infty} d\omega J(\omega) n(\omega) \times \int_0^\infty d\tau e^{i\omega\tau} [\tilde{c}_\alpha(t-\tau, t)\rho, c_\alpha] + \text{H.c.}, \quad (16)$$

where H.c. is the hermitian conjugate,

$$n(\omega) = \frac{1}{e^{\hbar\omega/k_B T} - 1} \quad (17)$$

is the Bose-Einstein distribution. The operator \tilde{c}_α is defined as

$$\tilde{c}_\alpha(t, t_0) = [U_S(t, t_0)]^\dagger c_\alpha U_S(t, t_0) \quad (18)$$

and depends on the driving amplitude F via the time evolution operator in Eq. (14). In order to simplify the master equation further we take advantage of the fact that there exists a complete set of exact solutions to the isolated system dynamics. The details of the derivation are given in Appendix B. We find

$$\begin{aligned} \dot{\rho} = & -\frac{i}{\hbar} [H_S^F(t), \rho] \\ & + \left\{ \mathcal{S}_1^\alpha(t) [A(t)\rho A^\dagger(t) - A^\dagger(t)A(t)\rho] \right. \\ & + \mathcal{S}_2^\alpha(t) [A^\dagger(t)\rho A(t) - A(t)A^\dagger(t)\rho] \\ & + \mathcal{S}_3^\alpha(t) [A(t)\rho A(t) - A(t)A(t)\rho] \\ & + \mathcal{S}_4^\alpha(t) [A^\dagger(t)\rho A^\dagger(t) - A^\dagger(t)A^\dagger(t)\rho] \\ & \left. + \text{H.c.} \right\}, \quad (19) \end{aligned}$$

where the time-dependent functions \mathcal{S}_i^α ($i \in \{1, 2, 3, 4\}$) are defined in Appendix B. In order to be consistent with the separation of time-scales required by the Markov approximation [26, 50, 51], the definitions of \mathcal{S}_i^α ($i \in \{1, 2, 3, 4\}$) involve a time average to exclude any dynamic faster than the bath response time [see Eq. (B19)]. In this way we avoid tracking all the degeneracies in the Floquet eigenenergies [27, 52].

We show in Sec. III that Eq. (19) can be approximated by a simpler master equation in the high-temperature regime, which we refer to as high-temperature master equation (HTME). The HTME is obtained by ignoring the driving term in Eq. (18) which results in

$$\tilde{c}_\alpha(t, t_0) \rightarrow e^{\frac{i}{\hbar} H_S^0(t-t_0)} c_\alpha e^{-\frac{i}{\hbar} H_S^0(t-t_0)}. \quad (20)$$

With this additional approximation, the HTME for the Ohmic bath can be written as

$$\begin{aligned} \dot{\rho} = & -\frac{i}{\hbar} [H_S^F(t), \rho] \\ & + \left\{ \frac{\gamma}{2} n(\omega_0) [a^\dagger \rho, a] + \frac{\gamma}{2} (n(\omega_0) + 1) [a\rho, a^\dagger] \right. \\ & + \frac{\gamma}{2} n(\omega_0) e^{i2\alpha} [a^\dagger \rho, a^\dagger] \\ & \left. + \frac{\gamma}{2} (n(\omega_0) + 1) e^{-i2\alpha} [a\rho, a] + \text{H.c.} \right\}, \quad (21) \end{aligned}$$

where a^\dagger and a are the familiar creation and annihilation operators of the undriven harmonic oscillator. For an undriven system ($F = 0$) Eq. (21) reduces to the standard quantum optical master equation after a rotating wave approximation that eliminates all the terms in the third and fourth lines.

III. RESULTS

Here we present a systematic study of the quasi-steady state of the driven harmonic oscillator as a function of the

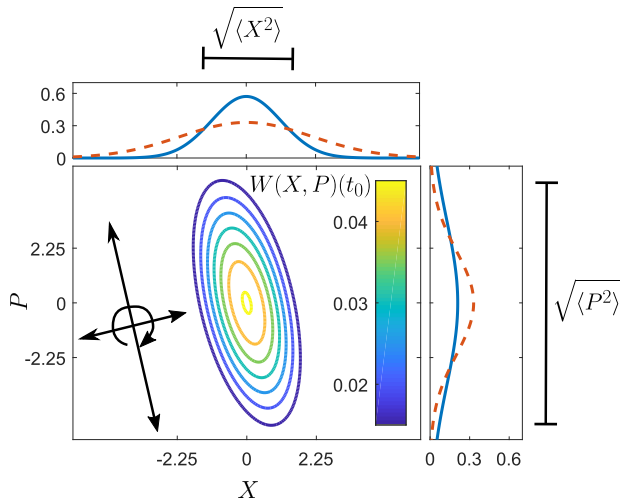


FIG. 2. (Color online) The central panel shows a snapshot of $W(X, P)$ at time $t_0 \gg 1/\gamma$. The black arrow next to the ellipse indicates its dynamics consisting of simultaneous squeezing and rotation. The top and right panel contain the resulting probability distributions of the quadratures X and P (blue solid line). The red dashed line in the side panels corresponds to the initial thermal state for $t < 0$. The width of the probability distribution is given by $\sqrt{\langle Y^2 \rangle}$ with $Y = X, P$. Driving parameters are $b = 0.1$, $q = 0.5$ and $\zeta = 0.7$ as defined in the text.

external driving parameters, the temperature of the bath and the coupling angle α in the system-bath Hamiltonian. In a first step, we describe how we characterise the quasi-steady state of the oscillator in Sec. III A. The numerical results are shown in Sec. III B.

We introduce dimensionless parameters which are frequently used to characterise periodically driven systems [53–55]. For the specific model at hand, $b = (2\omega_0/\omega_L)^2$ is proportional to the ratio of natural and driving frequencies squared and $q = 2F\omega_0^2/\omega_L^2$ characterises the effective driving strength. Throughout this work, we set the decay rate to $\gamma/\omega_0 = 0.02$ in order to be consistent with the Born Markov approximation. Note that γ enters the master equation (19) implicitly via the spectral density in Eq. (15). We further define $\zeta = \hbar\omega_0/(k_B T)$, which is proportional to the inverse temperature.

A. Observables

A descriptive way to illustrate the quantum state of the oscillator is given by the Wigner quasi probability distribution defined as [56, 57]

$$W(X, P)(t) = \frac{1}{\pi} \int_{-\infty}^{\infty} \langle X + Y | \rho(t) | X - Y \rangle e^{-2iPY/\hbar} dY. \quad (22)$$

In this equation, the density operator $\rho(t)$ is determined by Eq. (19) and X and P are dimensionless position and

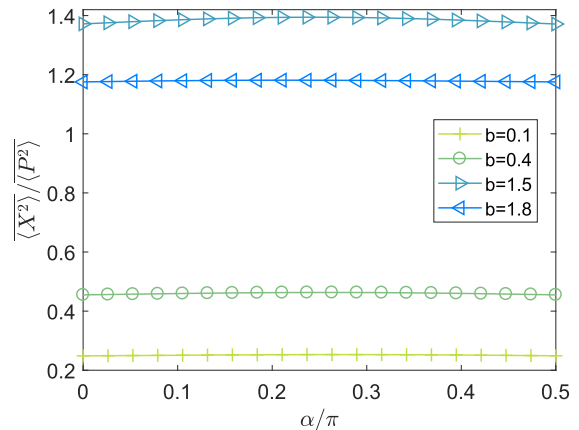


FIG. 3. (Color online) Ratio of the time averaged quadratures $\overline{\langle X^2 \rangle} / \overline{\langle P^2 \rangle}$ as a function of the coupling angle α and for different values of a . We have chosen $q = 0.5$, $\zeta = 10^{-4}$.

momentum operators, respectively,

$$X = \sqrt{\frac{m\omega_0}{\hbar}} x, \quad (23a)$$

$$P = \sqrt{\frac{1}{m\omega_0\hbar}} p. \quad (23b)$$

For $t < 0$ the system is in a thermal state, which corresponds to a circular quasi-probability distribution with equally sized position and momentum quadratures $\langle X^2 \rangle$ and $\langle P^2 \rangle$, respectively. Once the driving is switched on at $t = 0$, the shape of the Wigner function changes in time. A snapshot of $W(X, P)(t_0)$ at $t_0 \gg 1/\gamma$ is shown in Fig. 2. In contrast to the thermal distribution, $W(X, P)(t_0)$ has an elliptic shape with a tilted major axis. The value of $\langle X^2 \rangle$ ($\langle P^2 \rangle$) has decreased (increased) with respect to the thermal distribution. Even though this is just an example of the Wigner function at a particular point in time, the whole dynamics of $W(X, P)(t \gg 1/\gamma)$ can be described by an ellipse rotating around the origin with period $4\pi/\omega_L$. During one revolution the angular velocity of rotation changes in time, and the ellipse grows and shrinks along its major and minor axis.

The dynamics of $\{\langle X^2 \rangle, \langle P^2 \rangle, \langle XP + PX \rangle\}$ can be obtained from a closed set of equations since the total Hamiltonian H^α in Eq. (9) is quadratic and therefore preserves the Gaussian nature of the initial thermal state [58–63]. This set of equations is derived from the full master equation (19) and given in Appendix C. A similar closed set of equations can be obtained from the HTME in Eq. (21), and the corresponding results are denoted by $\langle \dots \rangle_{\text{HTME}}$. In the following we consider the steady state regime $t \gg 1/\gamma$ and restrict our analysis to $\overline{\langle X^2 \rangle}$ and $\overline{\langle P^2 \rangle}$, where the bar indicates a time average over the interval $\Delta t \approx 1/\gamma \gg 2\pi/\omega_L$. It follows that $\sqrt{\overline{\langle X^2 \rangle}}$ and $\sqrt{\overline{\langle P^2 \rangle}}$ characterise the width of the

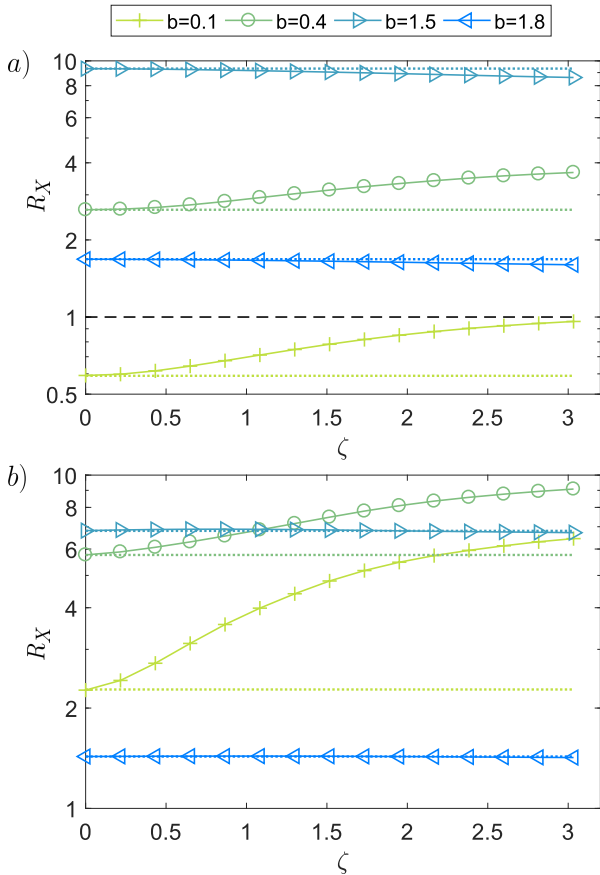


FIG. 4. (Color online) R_X as a function of inverse temperature ζ for $q = 0.5$, different driving frequencies and coupling angle a) $\alpha = 0$ and b) $\alpha = \frac{\pi}{2}$. Dotted lines of the same color indicate the results obtained from the evolution of the HTME. Dashed line at $R_X = 1$ in a) is a guide to the eye.

time-averaged Wigner function in X and P , respectively.

B. Numerical results

Here we systematically investigate the dependence of $\overline{\langle X^2 \rangle}$ and $\overline{\langle P^2 \rangle}$ on the parameters b , ζ and α . In a first step, we find that the ratio $\overline{\langle X^2 \rangle} / \overline{\langle P^2 \rangle}$ is approximately independent of the coupling angle α as shown in Fig. 3. This ratio only depends on the driving frequency and strength, and is larger (smaller) than unity for $b > 1$ ($b < 1$). The shape of the time-averaged Wigner function thus deviates significantly from a circle in the presence of the parametric driving. The results in Fig. 3 correspond to the high-temperature limit $\zeta = 10^{-4}$. However, we find that the ratio $\overline{\langle X^2 \rangle} / \overline{\langle P^2 \rangle}$ is also approximately independent of ζ for the considered range of values $\zeta \in [10^{-4}, 3]$.

The previously discussed dependence of $\overline{\langle X^2 \rangle}$ and $\overline{\langle P^2 \rangle}$ allows us to restrict the following analysis to one of the two quadratures. We choose $\overline{\langle X^2 \rangle}$ and investigate its

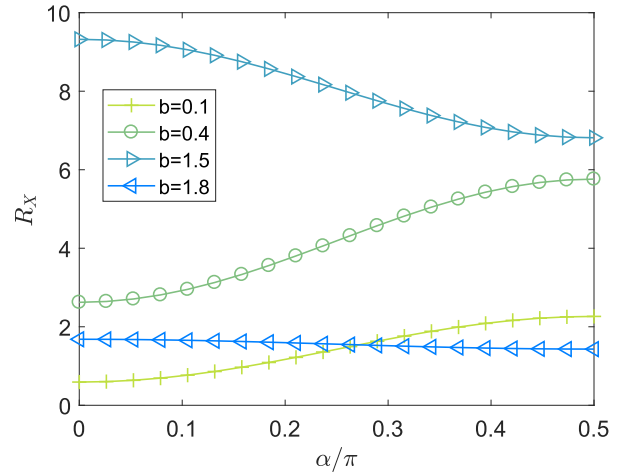


FIG. 5. (Color online) R_X as a function of coupling angle α for different values of a , driving strength $q = 0.5$ and inverse temperature $\zeta = 10^{-4}$.

dependence on b , α and ζ by introducing the short-hand notation

$$R_X = \overline{\langle X^2 \rangle} / \langle X^2 \rangle_{\text{thermal}}, \quad (24)$$

where $\langle X^2 \rangle_{\text{thermal}}$ is the undriven initial thermal value of $\langle X^2 \rangle$. A value of $R_X > 1$ [$R_X < 1$] thus means that the driving enhances [reduces] the value of $\overline{\langle X^2 \rangle}$ compared to its thermal value.

The dependence of R_X on ζ is shown in Figs. 4a) and b) for position and momentum coupling, respectively. Note that all values for R_X in Fig. 4 differ from unity and hence the parametric driving changes the value of $\overline{\langle X^2 \rangle}$ compared to $\langle X^2 \rangle_{\text{thermal}}$. Furthermore, we note that the results for R_X in Fig. 4 differ significantly for position and momentum coupling. Most prominently, $R_X > 1$ for all curves in Fig. 4b) (momentum coupling), while $R_X < 1$ for position coupling and $b = 0.1$. The reduction of $(R_X)_{\zeta \rightarrow 0}$ below unity for position coupling and fast driving ($b \ll 1$) has already been studied in Refs. [58, 64–66]. In general, we find that R_X strongly increases with ζ for both coupling types if $b < 1$. On the other hand, R_X shows a much weaker dependence on ζ for $b > 1$. The value of $(R_X)_{b > 1}$ slightly decreases with ζ for position coupling and remains approximately constant for momentum coupling.

In order to illustrate the significance of the ζ -dependence of R_X , we show the results for $(R_X)_{\text{HTME}}$ obtained via the HTME in Eq. (21) by the horizontal dotted lines in Fig. 4. Since they exhibit no ζ -dependence, the temperature dependence of R_X predicted by the full master equation is a direct consequence of the parametric driving on the system-bath coupling. The differences between the HTME and full master equation are most pronounced near $\zeta = 3$ and for $b = 0.1$. On the other hand, we find that R_X converges to $(R_X)_{\text{HTME}}$ in the limit $\zeta \rightarrow 0$ which can be understood as follows. The thermal

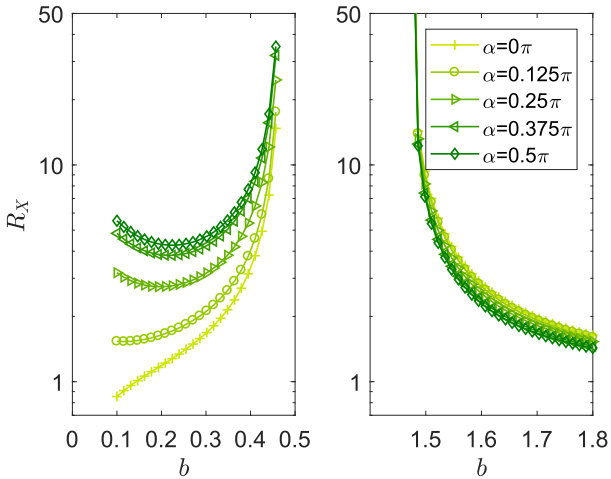


FIG. 6. (Color online) R_X as a function of inverse driving frequencies for different coupling angles α , driving strength $q = 0.5$ and inverse temperature $\zeta = 2$. The left and right panel correspond to driving above and below the resonance frequency, respectively.

correlation time of the bath $\tau_B = \hbar/(2\pi k_B T)$ [26, 51] becomes much smaller than the typical timescale $\tau_S = \min(1/\omega_0, 1/\omega_L)$ of the system dynamics in the high-temperature limit. Consequently, the time-evolution of the system cannot influence the system-bath coupling.

Next we investigate the α -dependence of R_X in the high-temperature limit and for different driving frequencies. The results are shown in Fig. 5. We observe an increase (decrease) of R_X with increasing α for $b < 1$ ($b > 1$). This behaviour is similar to the functional dependence of R_X on ζ and b shown in Fig. 4. We thus find that increasing α or ζ leads to qualitatively comparable effects. Most importantly, R_X shows a strong dependence on α for $b = 0.4$ and $b = 1.5$. Since R_X is monotonously increasing (decreasing) for $b = 0.4$ ($b = 1.5$), one can determine the coupling angle α by comparing $\overline{\langle X^2 \rangle}$ to $\langle X^2 \rangle_{\text{thermal}}$.

The α -dependence of the results in Fig. 5 are a direct consequence of the counter-rotating terms $\propto e^{\pm 2i\alpha}$ in the HTME in Eq. (21). If the counter-rotating terms in the HTME are neglected within a rotating-wave approximation, it is independent of α . Such a rotating-wave approximation is justified, e.g., for the undriven oscillator and hence we conclude that the α -dependence is a direct consequence of the driving.

In order to identify the parameter regime with the strongest α -dependence, we move away from the high-temperature limit and show R_X as a function of b for different values of α in Fig. 6. Here the left and right panels correspond to the parameter range $b < 0.5$ and $b > 1.45$, respectively. For values closer to $b = 1$ the solutions become unstable and no steady state can be achieved. Figure 6 shows that R_X exhibits the strongest dependence on α for $b \approx 0.1$. In particular, note that the

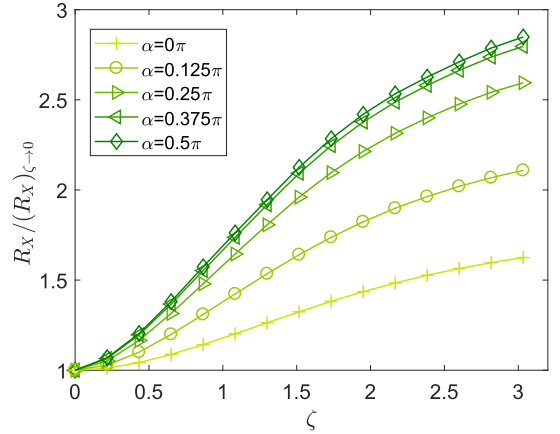


FIG. 7. (Color online) $R_X/(R_X)_{\zeta \rightarrow 0}$ as a function of ζ for $b = 0.1$, $q = 0.5$ and different values of α . The values of $(R_X)_{\zeta \rightarrow 0}$ can be obtained from the $b = 0.1$ curve in Fig. 5.

range of the R_X values from $\alpha = 0$ to $\alpha = \pi/2$ is larger than in the corresponding curve for $b = 0.1$ in Fig. 5 due to the different ζ values.

Finally, we focus on $b = 0.1$ and investigate the ζ -dependence of R_X for different values of α . We find that R_X increases relative to its $\zeta \rightarrow 0$ value for all considered values of α as shown in Fig. 7. The relative increase with ζ is the largest for $\alpha = \pi/2$ and the smallest for $\alpha = 0$. Furthermore, we find that small changes in α change the ζ -dependence of $R_X/(R_X)_{\zeta \rightarrow 0}$ most significantly near $\alpha = 0$.

Two conclusions can be drawn from the results in Fig. 7. First, increasing the value of ζ increases the spread of R_X with α . It thus becomes easier to determine α via a comparison of $\overline{\langle X^2 \rangle}$ and $\langle X^2 \rangle_{\text{thermal}}$ for smaller temperatures of the bath. Second, the difference of the ζ -dependence of R_X for various choices of α opens up a second route to determining α . For example, one could increase ζ by a given factor and measure the corresponding increase in R_X . According to Fig. 7, this increase is a unique function of α . Note that this approach works best for small α where the ζ -dependence of R_X is most sensitive to changes in α .

IV. DISCUSSION OF α -DEPENDENCE

The aim of this section is to give an intuitive picture for the strong α -dependence of the results in Sec. III B. To this end we show in Appendix D that the total Hamiltonian H^α in Eq. (9) is unitarily equivalent to

$$\mathcal{H}^\alpha = H_S^F(t) + H_B + \mathcal{H}_I^\alpha + H_{\text{shift}}, \quad (25)$$

where $H_S^F(t)$ and H_B remain unchanged and H_{shift} is given in Appendix D. The latter term describes small shifts of the bath and system frequencies and will be neglected in the following. The transformed interaction

Hamiltonian \mathcal{H}_I^α is given by

$$\mathcal{H}_I^\alpha = -xB^\alpha, \quad (26)$$

where

$$B^\alpha = \sum_{r=1}^N \kappa_r \left(\cos(\alpha)x_r - \frac{\sin(\alpha)}{m_r\omega_0} p_r \right). \quad (27)$$

In contrast to H_I^α in Eq. (6), the system-bath coupling in \mathcal{H}_I^α is mediated by the position coordinate of the oscillator coupled to an α -dependent superposition of position and momentum operators of the bath modes. In this way, the α -dependence has been entirely moved from the coupling operator to the bath.

Following the steps in Appendix B we derive a master equation for the density operator ρ_U from the transformed Hamiltonian \mathcal{H}^α , see Appendix D. We have explicitly verified that ρ_U and ρ lead to the same results for all parameters investigated in Sec. III B. In the derivation of the master equation for ρ_U , the linear superposition of bath operators in Eq. (27) gives rise to an α -dependent spectral density

$$J^\alpha(\omega) = J(\omega) \left[\cos(\alpha)^2 + \left(\frac{\omega}{\omega_0} \right)^2 \sin^2(\alpha) \right], \quad (28)$$

which is the product of the Ohmic spectral density $J(\omega)$ in Eq. (15) and an α -dependent function. We show $J^\alpha(\omega)$ for the two extreme cases $\alpha = 0$ and $\alpha = \pi/2$ in Fig. 8. While $J^0(\omega)$ and $J^{\pi/2}(\omega)$ are identical at $\omega = \pm\omega_0$, they differ significantly for $|\omega| \neq \omega_0$.

We are now in a position to understand the α -dependence of the results in Sec. III B. In general, the system-bath interaction is determined by the values of $J^\alpha(\omega_c)$ at the characteristic frequencies ω_c of the classical solution of the undamped harmonic oscillator [see Appendix E for details]. We have found that all observables in Sec. III B are independent of α for an undriven oscillator. In this case, the resonance frequency ω_0 is the only characteristic frequency involved in the system dynamics. However, the spectral density in Eq. (28) satisfies $J^\alpha(\pm\omega_0) = J(\pm\omega_0)$ for all α , and hence the system-bath interaction is independent of α .

This picture changes significantly if the driving is switched on. The driving leads to new characteristic frequencies $\omega_c = \pm\mu + r\omega_L$, with $r \in \mathbb{Z}$ and where μ is the quasi-frequency of the Floquet spectrum closest to ω_0 of the underlying classical model of a driven but undamped harmonic oscillator. Since the spectral density J^α depends strongly on α for $|\omega| > \omega_0$ [see Fig. 8], the parametric driving leads to α -dependent results.

V. SUMMARY AND CONCLUSION

We have shown that parametric driving of a harmonic oscillator coupled to a heat bath allows one to distinguish

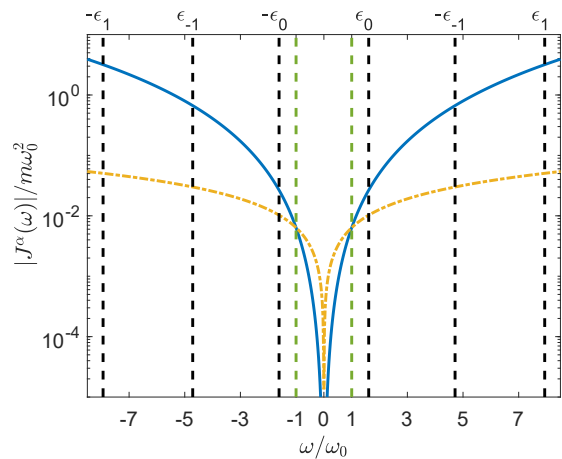


FIG. 8. (Color online) The dash-dotted yellow (solid blue) line corresponds to the bath spectral density $J^{\alpha=0}(\omega)$ [$J^{\alpha=\pi/2}(\omega)$]. The green dashed vertical lines mark the undriven system frequency $\pm\omega_0$. The scaled Floquet quasi-frequencies $\epsilon_r = (\mu + r\omega_L)/\omega_0$ for $q = 0.5$ and $b = 0.1$ are indicated by black dashed vertical lines.

between different microscopic models for the system-bath interaction. More specifically, we have considered a bath with an Ohmic spectral density that couples to a linear superposition of the position and momentum degrees of freedom of the oscillator. This superposition is parametrised via the coupling angle α which allows one to continuously change the character of the coupling from position to momentum coupling. We have systematically investigated the dependence of the time-averaged expectation values of $\langle X^2 \rangle$ and $\langle P^2 \rangle$ on the driving parameters, temperature T of the bath and α . While $\langle X^2 \rangle / \langle P^2 \rangle$ is approximately independent of α and T , we have shown that $R_X = \langle X^2 \rangle / \langle X^2 \rangle_{\text{thermal}}$ shows a strong dependence on temperature and on the coupling angle α . This dependence on the coupling angle could be used to determine α by measuring $\langle X^2 \rangle$ ($\langle X^2 \rangle_{\text{thermal}}$ in the presence (absence) of the parametric driving. We have found that R_X exhibits the strongest dependence on α for large driving frequencies $\omega_L \gg \omega_0$ and for bath temperatures with $k_B T \leq \hbar\omega_0$. In this regime, R_X also displays a characteristic dependence on inverse temperature for each value of α , thus offering an additional route to determine the value of α in the interaction Hamiltonian.

Our results have been obtained within the framework of a master equation in Born-Markov approximation that accounts for the modification of the system-bath interaction due to the parametric driving. In order to be consistent with the Markov approximation, we describe the time evolution of the reduced density operator of the oscillator on a coarse-grained time axis with resolution Δt , where Δt is much smaller than $1/\gamma$ and much larger than the bath correlation time. We compare our results to a simpler master equation that neglects the influence of the driving on the dissipative part and where all counter-rotating terms are kept. We find that this HTME agrees

with the full master equation in the high-temperature limit where $\hbar\omega_0 \ll k_B T$, but deviates significantly otherwise. We thus conclude that the influence of the parametric driving on the system-bath coupling must be taken into account in general.

We have shown that the α -dependence of our results can be understood in an intuitive way by applying a unitary transformation to the total system-bath Hamiltonian. In this transformed picture, the position variable of the oscillator couples to an α -dependent superposition of bath variables which results in an α -dependent spectral density J^α . Since the system-bath coupling is determined by the values of J^α at the Floquet quasi-frequencies associated with the parametric driving, the density operator obtained from this master equation depends on α if the system is driven.

Our results open up several directions for future investigations. The explanation of the α -dependence of our results via the unitarily equivalent model giving rise to an α -dependent spectral density shows that strong parametric driving allows one to probe an unknown spectral density if the microscopic coupling mechanism between the system and the bath is known. Furthermore, this approach could be extended to investigate systems with several competing dissipation mechanisms or to the non-Markovian regime of strong damping which is often encountered in solid-state materials. This could either be achieved by using the Feynman-Vernon path integral formalism [58] or the stochastic Liouville-von Neumann equation [67]. Eventually, an improved understanding of system-bath interactions in these systems paves the way to control and engineer their quantum dynamics via strong driving. For example, cooling of a driven harmonic oscillator coupled to a non-Markovian bath can be achieved via optimal control techniques [63, 68]. This could allow one to prepare the oscillator in non-classical, squeezed states [69–72].

ACKNOWLEDGMENTS

MK thanks the National Research Foundation and the Ministry of Education of Singapore for support. The research leading to these results has received funding from the European Research Council under the European Unions Seventh Framework Programme (FP7/2007-2013)/ERC Grant Agreement no. 319286 Q-MAC and from EPSRC programme grant EP/P009565/1 DesOEq.

Appendix A: Exact solution of the driven harmonic oscillator

Here we describe the exact solutions $\psi_n(x, t)$ to the time-dependent Schrödinger equation in Eq. (3) following the approach in [44, 45] that is based on dynamical

invariants [39, 73]. We write the solutions as

$$\psi_n(x, t) = \frac{1}{\sqrt{2^n n!}} \left(\frac{m\omega_I}{\pi \hbar g_-(t)} \right)^{\frac{1}{4}} e^{-i \frac{g_0(t)}{2\hbar g_-(t)} x^2} e^{-i\Lambda(t)(n+\frac{1}{2})} e^{-\frac{m\omega_I}{2\hbar g_-(t)} x^2} H_n \left(\sqrt{\frac{m\omega_I}{\hbar g_-(t)}} x \right), \quad (\text{A1})$$

where

$$\Lambda(t) = \int_0^t dt' \frac{\omega_I}{g_-(t')}, \quad (\text{A2})$$

is a global phase,

$$\omega_I = \frac{1}{m} \sqrt{g_+(t)g_-(t) - g_0^2(t)}, \quad (\text{A3})$$

is a time-independent constant frequency and H_n are the Hermite polynomials of degree n . The functions $g_+(t)$, $g_-(t)$ and $g_0(t)$ in Eq. (A1) are defined as

$$g_+(t) = m^2 \dot{f}_1(t) \dot{f}_2(t), \quad (\text{A4a})$$

$$g_0(t) = -\frac{m}{2} [\dot{f}_1(t) f_2(t) + f_1(t) \dot{f}_2(t)], \quad (\text{A4b})$$

$$g_-(t) = f_1(t) f_2(t), \quad (\text{A4c})$$

where $f_i(t)$ ($i \in \{1, 2\}$) are two linearly independent solutions of the classical harmonic oscillator. These functions obey

$$\ddot{f}_i(t) + \omega^2(t) f_i(t) = 0, \quad (\text{A5})$$

and we impose the initial condition $f_i(0) = 1$ at $t = 0$ and require $f_1(t) = f_2(t)^*$. For $t < 0$ where the driving is absent we thus find $f_{1,2}(t < 0) = e^{\pm i\omega_0 t}$, and consequently $g_0(t < 0) = 0$. Furthermore, as $g_-(t < 0) = 1$ the chosen initial conditions result in $\omega_I = \omega_0$ such that $\psi_n(x, t)$ reduces to the harmonic oscillator eigenstates. These states form an orthogonal basis and the states $\psi_n(x, t)$ remain orthogonal for $t \geq 0$, i.e. $\langle \psi_n(t) | \psi_m(t) \rangle = \delta_{n,m}$ as the time dependence of the argument $\frac{m\omega_I}{\hbar g_-(t)}$ of the integral in the equal time norm can be eliminated by a change of variables. It follows that the states $|\psi_n(t)\rangle$ in Eq. (A1) span a complete basis at all times.

We define generalised creation and annihilation operators A^\dagger and A that act on the states $|\psi_n(t)\rangle$ as described in Eq. (4). The annihilation operator is given by [28]

$$A(t) = \frac{1}{\sqrt{2}} \left[\sqrt{\frac{m\omega_0}{\hbar}} h_1(t) x + \sqrt{\frac{1}{\hbar m \omega_0}} h_2(t) p \right], \quad (\text{A6})$$

and the complex functions $h_1(t)$ and $h_2(t)$ are defined as

$$h_1(t) = \exp(i\Lambda(t)) \sqrt{\frac{\omega_I}{\omega_0 g_-(t)}} \left(1 + i \frac{g_0(t)}{m\omega_I} \right), \quad (\text{A7a})$$

$$h_2(t) = i \exp(i\Lambda(t)) \sqrt{\frac{\omega_0 g_-(t)}{\omega_I}}. \quad (\text{A7b})$$

Since $[x, p] = i\hbar$ and $h_1(t)h_2^*(t) - h_1^*(t)h_2(t) = -2i$, the equal-time commutation relation $[A(t), A^\dagger(t)] = 1$ is satisfied.

Appendix B: Master equation derivation

Here we discuss the derivation of the master equation in Sec. II B. Our approach builds on the work presented in [28], but considers a more general system-bath coupling, does not use the Floquet basis states and employs the weakest possible rotating-wave approximation in order to be consistent with the Born-Markov approximation.

In a first step we re-write the dissipative term $\mathcal{K}\rho$ in Eq. (11) as follows [26, 27, 52],

$$\mathcal{K}\rho = \frac{1}{\hbar^2} \int_0^\infty d\tau \left(\frac{i}{2} D(\tau) [c_\alpha, \{\tilde{c}_\alpha(t-\tau, t), \rho\}] - \frac{1}{2} D_1(\tau) [c_\alpha, [\tilde{c}_\alpha(t-\tau, t), \rho]] \right), \quad (\text{B1})$$

where $\{Q, W\} = QW + WQ$ is the anti-commutator for operators Q, W and we introduced following [26] the dissipation kernel

$$D(\tau) = i \langle [B, \tilde{B}(-\tau)] \rangle = i [B, \tilde{B}(-\tau)], \quad (\text{B2})$$

and the noise kernel

$$D_1(\tau) = \langle \{B, \tilde{B}(-\tau)\} \rangle. \quad (\text{B3})$$

We find

$$D(\tau) = 2\hbar \int_0^\infty d\omega J(\omega) \sin \omega\tau, \quad (\text{B4a})$$

$$D_1(\tau) = 2\hbar \int_0^\infty d\omega J(\omega) \coth(\hbar\omega/2k_B T) \cos \omega\tau, \quad (\text{B4b})$$

and

$$J(\omega) = \sum_{n=1}^N \frac{\kappa_n^2}{2m_n\omega_n} \delta(\omega - \omega_n) \quad (\text{B5})$$

is the spectral density. As described in the main text we assume that $J(\omega)$ is Ohmic with a Lorentz-Drude cutoff as given in Eq. (15). The longest thermal correlation time is then given by $\tau_B = \max[\hbar/(2\pi k_B T), \Omega^{-1}]$. We set $\Omega = 10^5 \omega_0$ such that for all considered parameters $\tau_B = \hbar/(2\pi k_B T)$. With the identities $J(\omega) = -J(-\omega)$ as well as $-n(-\omega) = n(\omega) + 1$ we obtain Eq. (16).

The solution of the master equation (10) with $\mathcal{K}\rho$ as in Eq. (16) is greatly simplified by projecting it onto the states $|\psi_n(t)\rangle$ which solve the full Schrödinger equation of the driven oscillator. The matrix elements of the density operator of the system in this basis are denoted by

$$\rho_{nm}(t) = \langle \psi_n(t) | \rho(t) | \psi_m(t) \rangle, \quad (\text{B6})$$

and evolve only due to the system-bath coupling. We find

$$\dot{\rho}_{nm}(t) = \sum_{k,l} [\bar{C}_{nk}^\alpha(t) \rho_{kl}(t) C_{lm}^\alpha(t) - C_{nk}^\alpha(t) \bar{C}_{kl}^\alpha(t) \rho_{lm}(t)] + \text{H.c.}, \quad (\text{B7})$$

where

$$C_{nm}^\alpha(t) = \langle \psi_n(t) | c_\alpha | \psi_m(t) \rangle, \quad (\text{B8a})$$

$$\bar{C}_{nm}^\alpha(t) = \frac{1}{\hbar} \int_{-\infty}^\infty d\omega J(\omega) n(\omega) \times \int_0^\infty d\tau e^{i\omega\tau} C_{nm}^\alpha(t-\tau). \quad (\text{B8b})$$

In order to evaluate these matrix elements, we express the coupling operator c_α in Eq. (7) in terms of the generalised creation and annihilation operators $A(t)$ and $A^\dagger(t)$,

$$c_\alpha = s_1^\alpha(t) A^\dagger(t) + s_2^\alpha(t) A(t), \quad (\text{B9})$$

where

$$s_1^\alpha(t) = i\sqrt{\frac{\hbar}{2m\omega_0}} [\sin(\alpha)h_1(t) - \cos(\alpha)h_2(t)] \quad (\text{B10})$$

is a complex-valued function and $s_2^\alpha(t) = [s_1^\alpha(t)]^*$. The matrix element in Eq. (B8a) thus reads

$$C_{nm}^\alpha(t) = s_1^\alpha(t) A_{nm}^\dagger + s_2^\alpha(t) A_{nm}, \quad (\text{B11})$$

and the time-independent matrix elements of the creation and annihilation operators are given by

$$A_{nm}^\dagger = \langle \psi_n(t) | A^\dagger(t) | \psi_m(t) \rangle = \sqrt{m+1} \delta_{n,m+1}, \quad (\text{B12a})$$

$$A_{nm} = \langle \psi_n(t) | A(t) | \psi_m(t) \rangle = \sqrt{m} \delta_{n,m-1}. \quad (\text{B12b})$$

Next we discuss the evaluation of \bar{C}_{nm} in Eq. (B8b).

With the help of Eq. (B11), we find

$$\bar{C}_{nm}^\alpha(t) = \bar{s}_1^\alpha(t) A_{nm}^\dagger + \bar{s}_2^\alpha(t) A_{nm}, \quad (\text{B13})$$

where

$$\bar{s}_i^\alpha(t) = \frac{1}{\hbar} \int_{-\infty}^\infty d\omega J(\omega) n(\omega) \int_0^\infty d\tau e^{i\omega\tau} s_i^\alpha(t-\tau). \quad (\text{B14})$$

In order to evaluate Eq. (B14), we choose a sufficiently large time interval $[t_i, t_f]$ of length $T_{if} = t_f - t_i$ to avoid artefacts from the Gibbs effect [74] and represent s_i^α in terms of the first N_k terms of its discrete Fourier series,

$$s_i^\alpha(t_i < t < t_f) \approx \sum_{k=-k_{\max}}^{k_{\max}} \mathcal{F}[s_i^\alpha](\omega_k) e^{i\omega_k t}. \quad (\text{B15})$$

Here $\omega_k = \frac{2\pi k}{T_{if}}$ are the discrete frequencies with integer index k , $k_{\max} = \frac{N_k-1}{2}$ and the Fourier coefficients $\mathcal{F}[s_i^\alpha](\omega_k)$ are defined as

$$\mathcal{F}[s_i^\alpha](\omega_k) = \frac{1}{T_{if}} \int_{t_i}^{t_f} s_i^\alpha(t) e^{-i\omega_k t} dt. \quad (\text{B16})$$

The expansion in Eq. (B15) allows us to evaluate the integrals in Eq. (B14). We find

$$\bar{s}_i^\alpha(t) = \frac{\pi}{\hbar} \sum_{k=-k_{\max}}^{k_{\max}} J(\omega_k) n(\omega_k) e^{i\omega_k t} \mathcal{F}[s_i^\alpha](\omega_k), \quad (\text{B17})$$

where we employed the identity $\int_0^\infty dt e^{i\omega t} = \pi\delta(\omega) + P(i/\omega)$ and neglected the principal part.

We now return to the master equation (B7). Substituting Eqs. (B11) and (B13) in Eq. (B7) results in a differential equation for ρ_{nm} with time-dependent coefficients $s_i^\alpha(t)\bar{s}_j^\alpha(t)$. In order to be consistent with the Born-Markov approximation we average these time-dependent terms over the correlation time of the bath τ_B times a constant factor f . In order to make sure that the bath cannot introduce any dynamics faster than τ_B , we set $f = 10$ in Eq. (B19). This is necessary since the Markov approximation assumes that the system does not evolve appreciably over this time scale. We find

$$\begin{aligned} \dot{\rho}_{nm}(t) = & \sum_{k,l} \left\{ \mathcal{S}_1^\alpha(t) \left[A_{nk} \rho_{kl} A_{lm}^\dagger - A_{nk}^\dagger A_{kl} \rho_{lm} \right] \right. \\ & + \mathcal{S}_2^\alpha(t) \left[A_{nk}^\dagger \rho_{kl} A_{lm} - A_{nk} A_{kl}^\dagger \rho_{lm} \right] \\ & + \mathcal{S}_3^\alpha(t) \left[A_{nk} \rho_{kl} A_{lm} - A_{nk} A_{kl} \rho_{lm} \right] \\ & + \mathcal{S}_4^\alpha(t) \left[A_{nk}^\dagger \rho_{kl} A_{lm}^\dagger - A_{nk}^\dagger A_{kl}^\dagger \rho_{lm} \right] \\ & \left. \right\} + \text{H.c.}, \quad (\text{B18}) \end{aligned}$$

where

$$\mathcal{S}_1^\alpha(t) = \frac{1}{f\tau_B} \int_{t-f\tau_B}^t dt' \bar{s}_2^\alpha(t') s_1^\alpha(t'), \quad (\text{B19a})$$

$$\mathcal{S}_2^\alpha(t) = \frac{1}{f\tau_B} \int_{t-f\tau_B}^t dt' \bar{s}_1^\alpha(t') s_2^\alpha(t'), \quad (\text{B19b})$$

$$\mathcal{S}_3^\alpha(t) = \frac{1}{f\tau_B} \int_{t-f\tau_B}^t dt' \bar{s}_2^\alpha(t') s_2^\alpha(t'), \quad (\text{B19c})$$

$$\mathcal{S}_4^\alpha(t) = \frac{1}{f\tau_B} \int_{t-f\tau_B}^t dt' \bar{s}_1^\alpha(t') s_1^\alpha(t'). \quad (\text{B19d})$$

By converting Eq. (B18) into an operator-valued equation we obtain Eq. (19) in the main text.

Appendix C: Closed set of equations of motions for full master equation

A closed set of differential equations for the components of the the vector $\mathbf{v} = (\langle X^2 \rangle, \langle P^2 \rangle, \langle XP + PX \rangle)^\top$

with position-momentum correlator $D = XP + XP$ can be derived from the full master equation and is given by

$$\begin{aligned} \frac{d}{dt} v_1 = & \omega_0 v_3 \\ & + \left\{ -iv_1 [h_1(h_2^* S_1^\alpha + h_2 S_3^\alpha) + h_1^*(h_2 S_2^\alpha + h_2^* S_4^\alpha)] \right. \\ & \left. - \frac{iv_3 + 1}{2} [h_2(h_2^* S_1^\alpha + h_2 S_3^\alpha) + h_2^*(h_2 S_2^\alpha + h_2^* S_4^\alpha)] + \text{h.c.} \right\}, \quad (\text{C1}) \end{aligned}$$

$$\begin{aligned} \frac{d}{dt} v_2 = & -\frac{\omega^2(t)}{\omega_0} v_3 \\ & + \left\{ iv_2 [h_2(h_1^* S_1^\alpha + h_1 S_3^\alpha) + h_2^*(h_1 S_2^\alpha + h_1^* S_4^\alpha)] \right. \\ & \left. + \frac{iv_3 + 1}{2} [h_1(h_1^* S_1^\alpha + h_1 S_3^\alpha) + h_1^*(h_1 S_2^\alpha + h_1^* S_4^\alpha)] + \text{h.c.} \right\}, \quad (\text{C2}) \end{aligned}$$

and

$$\begin{aligned} \frac{d}{dt} v_3 = & 2\omega_0 v_2 - 2\frac{\omega^2(t)}{\omega_0} v_1 \\ & + \left\{ iv_1 [h_1(h_1^* S_1^\alpha + h_1 S_3^\alpha) + h_1^*(h_1 S_2^\alpha + h_1^* S_4^\alpha)] \right. \\ & - iv_2 [h_2(h_2^* S_1^\alpha + h_2 S_3^\alpha) + h_2^*(h_2 S_2^\alpha + h_2^* S_4^\alpha)] \\ & - \frac{1}{2} [(h_1^* h_2 + h_2^* h_1)(S_1^\alpha + S_2^\alpha) + 2h_1 h_2 S_3^\alpha + 2h_1^* h_2^* S_4^\alpha] \\ & \left. - v_3 [S_1^\alpha - S_2^\alpha] + \text{h.c.} \right\}. \quad (\text{C3}) \end{aligned}$$

In case of the HTME, we obtain

$$\frac{d\mathbf{v}}{dt} = M_i^\alpha \mathbf{v} + A_w \cos(\omega_L t) M_t \mathbf{v} + \mathbf{I}_\alpha, \quad (\text{C4})$$

where

$$\begin{aligned} M_i^\alpha & \quad (\text{C5}) \\ = & \begin{pmatrix} -2\gamma \sin^2(\alpha) & 0 & \frac{\gamma}{2} \sin(2\alpha) + \omega_0 \\ 0 & -2\gamma \cos^2(\alpha) & \frac{\gamma}{2} \sin(2\alpha) - \omega_0 \\ \gamma \sin(2\alpha) - 2\omega_0 & \gamma \sin(2\alpha) + 2\omega_0 & -\gamma \end{pmatrix} \end{aligned}$$

determines the isolated system dynamics,

$$M_t = \begin{pmatrix} 0 & 0 & 0 \\ 0 & 0 & -\omega_0 \\ -2\omega_0 & 0 & 0 \end{pmatrix} \quad (\text{C6})$$

accounts for the external driving and

$$\mathbf{I}_\alpha = [2n(\omega_0) + 1]\gamma \begin{pmatrix} \sin^2(\alpha) \\ \cos^2(\alpha) \\ -\sin(2\alpha) \end{pmatrix} \quad (\text{C7})$$

is the inhomogeneity in Eq. (C4).

Appendix D: Unitary transformation leading to \mathcal{H}^α

The unitary transformation relating the total Hamiltonian H^α to \mathcal{H}^α in Eq. (25) is given by

$$U = e^{-\frac{i}{\hbar} \frac{\sin(\alpha)}{\omega_0} x \sum_r \kappa_r x_r}. \quad (\text{D1})$$

This transformation leaves the position operators of the system and bath remain unchanged, i.e., $x_r = U^\dagger x_r U$ and $x = U^\dagger x U$. However, the momentum operators transform as

$$U^\dagger p_r U = p_r - \frac{\sin(\alpha)}{\omega_0} \kappa_r x, \quad (\text{D2a})$$

$$U^\dagger p U = p - \frac{\sin(\alpha)}{\omega_0} \sum_{r=1}^N \kappa_r x_r. \quad (\text{D2b})$$

The term $\mathcal{H}_{\text{shift}}$ in Eq. (25) is given by

$$\mathcal{H}_{\text{shift}} = \left[\frac{1}{2\omega_0^2} \sum_{r=1}^N \frac{\kappa_r^2}{m_r} x^2 - \frac{1}{2m\omega_0^2} \left(\sum_{r=1}^N \kappa_r x_r \right)^2 \right] \sin^2(\alpha). \quad (\text{D3})$$

Appendix E: Master equation resulting from \mathcal{H}^α

Following the steps in Appendix B, the transformed Hamiltonian \mathcal{H}^α gives rise to the following master equation,

$$\begin{aligned} \dot{\rho}_U = & -\frac{i}{\hbar} [H_S^F(t), \rho_U] \\ & + \left\{ \mathcal{U}_1^\alpha(t) [A(t)\rho_U A^\dagger(t) - A^\dagger(t)A(t)\rho_U] \right. \\ & + \mathcal{U}_2^\alpha(t) [A^\dagger(t)\rho_U A(t) - A(t)A^\dagger(t)\rho_U] \\ & + \mathcal{U}_3^\alpha(t) [A(t)\rho_U A(t) - A(t)A(t)\rho_U] \\ & + \mathcal{U}_4^\alpha(t) [A^\dagger(t)\rho_U A^\dagger(t) - A^\dagger(t)A^\dagger(t)\rho_U] \\ & \left. + \text{H.c.} \right\}, \quad (\text{E1}) \end{aligned}$$

where the operators A are the same as in Appendix B and

$$\mathcal{U}_1^\alpha(t) = \frac{1}{f\tau_B} \int_{t-f\tau_B}^t dt' \bar{u}_2^\alpha(t') u_1(t'), \quad (\text{E2a})$$

$$\mathcal{U}_2^\alpha(t) = \frac{1}{f\tau_B} \int_{t-f\tau_B}^t dt' \bar{u}_1^\alpha(t') u_2(t'), \quad (\text{E2b})$$

$$\mathcal{U}_3^\alpha(t) = \frac{1}{f\tau_B} \int_{t-f\tau_B}^t dt' \bar{u}_2^\alpha(t') u_2(t'), \quad (\text{E2c})$$

$$\mathcal{U}_4^\alpha(t) = \frac{1}{f\tau_B} \int_{t-f\tau_B}^t dt' \bar{u}_1^\alpha(t') u_1(t'). \quad (\text{E2d})$$

As in Appendix B, τ_B is the bath correlation time and $f = 10$. The function u_1 in Eq. (E2) is given by

$$u_1(t) = -i\sqrt{\frac{\hbar}{2m\omega_0}} h_2(t), \quad (\text{E3})$$

where $h_2(t)$ is defined in Eq. (A7) and only depends on the parameters of the classical parametric oscillator. Furthermore, $u_2(t) = [u_1(t)]^*$ and

$$\bar{u}_i^\alpha(t) = \frac{1}{\hbar} \int_{-\infty}^{\infty} d\omega J^\alpha(\omega) n(\omega) \int_0^{\infty} d\tau e^{i\omega\tau} u_i(t-\tau), \quad (\text{E4})$$

where J^α given in Eq. (28). By calculating the discrete Fourier transform $\mathcal{F}[u_i]$ of u_i and neglecting principle value integrals analogous to Eq. (B17), Eq. (E4) can be written as

$$\bar{u}_i^\alpha(t) \approx \frac{\pi}{\hbar} \sum_{k=-k_{\text{max}}}^{k_{\text{max}}} J^\alpha(w_k) n(w_k) e^{iw_k t} \mathcal{F}[u_i](w_k). \quad (\text{E5})$$

Since $u_1 \propto h_2$ and $u_2 \propto h_2^*$, Eq. (E5) shows that the system-bath interaction is determined by the spectral density $J^\alpha(w_k)$ evaluated at the characteristic frequencies $\omega_k = \omega_c$ of the classical harmonic oscillator solutions.

-
- [1] H. J. Metcalf and P. van der Straten, *Laser Cooling and Trapping* (Springer, New York, 1999).
- [2] M. Kiffner and M. J. Hartmann, Phys. Rev. A **81**, 021806(R) (2010).
- [3] M. Kiffner, U. Dörner, and D. Jaksch, Phys. Rev. A **85**, 023812 (2012).
- [4] S. Diehl, A. Tomadin, A. Micheli, R. Fazio, and P. Zoller, Phys. Rev. Lett. **105**, 015702 (2010).
- [5] M. Höning, M. Moos, and M. Fleischhauer, Phys. Rev. A **86**, 013606 (2012).
- [6] S. Diehl, A. Micheli, A. Kantian, B. Kraus, H. P. Büchler, and P. Zoller, Nat. Phys. **4**, 878 (2008).
- [7] M. Müller, S. Diehl, G. Pupillo, and P. Zoller, Adv. At. Mol. Opt. Phys. **61**, 1 (2012).
- [8] F. Verstraete, M. M. Wolf, and J. Ignacio Cirac, Nat. Phys. **5**, 633 (2009).
- [9] C. Capan, K. Behnia, Z. Z. Li, H. Raffy, and C. Marin, Phys. Rev. B **67**, 100507 (2003).
- [10] R. Mankowsky, B. Liu, S. Rajasekaran, H. Y. Liu, D. Mou, X. J. Zhou, R. Merlin, M. Först, and A. Cavalleri, Phys. Rev. Lett. **118**, 116402 (2017).
- [11] M. Först, R. I. Tobey, H. Bromberger, S. B. Wilkins, V. Khanna, A. D. Caviglia, Y.-D. Chuang, W. S. Lee, W. F. Schlotter, J. J. Turner, M. P. Minitti, O. Krupin, Z. J. Xu, J. S. Wen, G. D. Gu, S. S. Dhesi, A. Cavalleri, and J. P. Hill, Phys. Rev. Lett. **112**, 157002 (2014).
- [12] M. Först, A. Frano, S. Kaiser, R. Mankowsky, C. R. Hunt, J. J. Turner, G. L. Dakovski, M. P. Minitti, J. Robinson, T. Loew, M. Le Tacon, B. Keimer, J. P. Hill, A. Cavalleri, and S. S. Dhesi, Phys. Rev. B **90**, 184514 (2014).
- [13] T. F. Nova, A. Cartella, A. Cantaluppi, M. Först, D. Bossini, R. V. Mikhaylovskiy, A. V. Kimel, R. Merlin, and A. Cavalleri, Nat. Phys. **13**, 132 (2017).
- [14] A. D. Caviglia, R. Scherwitzl, P. Popovich, W. Hu, H. Bromberger, R. Singla, M. Mitrano, M. C. Hoffmann, S. Kaiser, P. Zubko, S. Gariglio, J.-M. Triscone, M. Först, and A. Cavalleri, Phys. Rev. Lett. **108**, 136801 (2012).
- [15] M. Först, A. D. Caviglia, R. Scherwitzl, R. Mankowsky, P. Zubko, V. Khanna, H. Bromberger, S. B. Wilkins, Y.-D. Chuang, W. S. Lee, W. F. Schlotter, J. J. Turner, G. Dakovski, M. P. Minitti, J. Robinson, S. R. Clark, D. Jaksch, J.-M. Triscone, J. P. Hill, S. S. Dhesi, and A. Cavalleri, Nat. Mater. **14**, 883 (2015).
- [16] M. Först, K. R. Beyerlein, R. Mankowsky, W. Hu, G. Mattoni, S. Catalano, M. Gibert, O. Yefanov, J. N. Clark, A. Frano, J. M. Glowia, M. Chollet, H. Lemke, B. Moser, S. P. Collins, S. S. Dhesi, A. D. Caviglia, J.-M. Triscone, and A. Cavalleri, Phys. Rev. Lett. **118**, 027401 (2017).
- [17] M. Rini, R. Tobey, N. Dean, J. Itatani, Y. Tomioka, Y. Tokura, R. W. Schoenlein, and A. Cavalleri, Nature **449**, 72 (2007).
- [18] M. Liu, H. Y. Hwang, H. Tao, A. C. Strikwerda, K. Fan, G. R. Keiser, A. J. Sternbach, K. G. West, S. Kittiwatanakul, J. Lu, S. A. Wolf, F. G. Omenetto, X. Zhang, K. A. Nelson, and R. D. Averitt, Nature **487**, 345 (2012).
- [19] S. J. Denny, S. R. Clark, Y. Laplace, A. Cavalleri, and D. Jaksch, Phys. Rev. Lett. **114**, 137001 (2015).
- [20] F. Schlawin, A. S. D. Dietrich, M. Kiffner, A. Cavalleri, and D. Jaksch, Phys. Rev. B **96**, 064526 (2017).
- [21] D. Fausti, R. I. Tobey, N. Dean, S. Kaiser, A. Dienst, M. C. Hoffmann, S. Pyon, T. Takayama, H. Takagi, and A. Cavalleri, Science **331**, 189 (2011).
- [22] W. Hu, S. Kaiser, D. Nicoletti, C. R. Hunt, I. Gierz, M. C. Hoffmann, M. Le Tacon, T. Loew, B. Keimer, and A. Cavalleri, Nat. Mater. **13**, 705 (2014).
- [23] M. Mitrano, A. Cantaluppi, D. Nicoletti, S. Kaiser, A. Perucchi, S. Lupi, P. Di Pietro, D. Pontiroli, M. Riccò, S. R. Clark, D. Jaksch, and A. Cavalleri, Nature **530**, 461 (2016).
- [24] S. Gröblacher, A. Trubarov, N. Prigge, G. D. Cole, M. Aspelmeyer, and J. Eisert, Nat. Commun. **6**, 7606 (2015).
- [25] R. Graham and R. Hubner, Ann. Phys. (N. Y.) **234**, 300 (1994).
- [26] H.-P. Breuer and F. Petruccione, *The Theory of Open Quantum Systems* (Oxford University Press, 2002).
- [27] R. Blümel, A. Buchleitner, R. Graham, L. Sirko, U. Smilansky, and H. Walther, Phys. Rev. A **44**, 4521 (1991).
- [28] S. Kohler, T. Dittrich, and P. Hänggi, Phys. Rev. E **55**, 300 (1997).
- [29] H.-P. Breuer and F. Petruccione, Phys. Rev. A **55**, 3101 (1997).
- [30] B. Donvil, arXiv: 1706.05235.
- [31] M. G. Floquet, Ann. Sci. l'É.N.S. **12**, 47 (1883).
- [32] J. H. Shirley, Phys. Rev. **138**, B979 (1965).
- [33] P. Hänggi, in *Quantum Transp. Dissipation*, edited by T. Dittrich, P. Hänggi, G.-L. Ingold, B. Kramer, G. Schön, and W. Zwerger (Wiley, 1997) Chap. 5.
- [34] S. Gasparinetti, P. Solinas, S. Pugnetti, R. Fazio, and J. P. Pekola, Phys. Rev. Lett. **110**, 150403 (2013).
- [35] C. F. Lo, Phys. Rev. A, At. Mol. Opt. Phys. **43**, 404 (1991).
- [36] C. F. Lo, Phys. Rev. A **47**, 115 (1993).
- [37] M. S. Abdalla and R. K. Colegrave, Phys. Rev. A **48**, 1526 (1993).
- [38] C. M. A. Dantas, I. A. Pedrosa, and B. Baseia, Phys. Rev. A **45**, 1320 (1992).
- [39] J.-Y. Ji, J. K. Kim, and S. P. Kim, Phys. Rev. A **51**, 4268 (1995).
- [40] D. Sheng, R. D. Khan, Z. Jialun, and S. Wenda, Int. J. Theor. Phys. **34**, 355 (1995).
- [41] D.-Y. Song, J. Phys. A: Math. Gen. **32**, 3449 (1999).
- [42] K. H. Yeon, K. K. Lee, C. I. Um, T. F. George, and L. N. Pandey, Phys. Rev. A **48**, 2716 (1993).
- [43] C.-I. Um, K.-H. Yeon, and T. F. George, Phys. Rep. **362**, 63 (2002).
- [44] J.-Y. Ji, J. K. Kim, S. P. Kim, and K.-S. Soh, Phys. Rev. A **52**, 3352 (1995).
- [45] I. A. Pedrosa, Phys. Rev. A **55**, 3219 (1997).
- [46] H. Kohler and F. Sols, Phys. A Stat. Mech. its Appl. **392**, 1989 (2013).
- [47] J.-D. Bao and Y.-Z. Zhuo, Phys. Rev. E **71**, 010102 (2005).
- [48] A. J. Leggett, Phys. Rev. B **30**, 1208 (1984).
- [49] A. Cuccoli, A. Fubini, V. Tognetti, and R. Vaia, Phys. Rev. E **64**, 066124 (2001).
- [50] U. Weiss, *Quantum Dissipative Systems*, 2nd ed. (World Scientific Publishing Co. Pte. Ltd., Singapore, 1999).
- [51] C. Gardiner and P. Zoller, *Quantum noise*, 2nd ed. (Springer, New York, 2000) p. 438.

- [52] D. W. Hone, R. Ketzmerick, and W. Kohn, *Phys. Rev. E* **79**, 051129 (2009).
- [53] M. Bukov, L. D'Alessio, and A. Polkovnikov, *Adv. Phys.* **64**, 139 (2015).
- [54] D. Leibfried, R. Blatt, C. Monroe, and D. Wineland, *Rev. Mod. Phys.* **75**, 281 (2003).
- [55] M. Abramowitz and I. A. Stegun, *Handbook of Mathematical Functions with Formulas, Graphs, and Mathematical Tables* (National Bureau of Standards Applied Mathematics Series, U.S. Government Printing Office, Washington, D.C., 1972).
- [56] E. Wigner, *Phys. Rev.* **40**, 749 (1932).
- [57] A. Polkovnikov, *Ann. Phys. (N. Y.)* **325**, 1790 (2010).
- [58] C. Zerbe and P. Hänggi, *Phys. Rev. E* **52**, 1533 (1995).
- [59] Y. Rezek and R. Kosloff, *New J. Phys.* **8**, 83 (2006).
- [60] J. Eisert and M. M. Wolf, in *Quantum Inf. with Continuous Var. Atoms Light* (Imperial College Press, 2007) pp. 23–42.
- [61] F. Galve, L. A. Pachón, and D. Zueco, *Phys. Rev. Lett.* **105**, 180501 (2010).
- [62] K. W. Chang and C. K. Law, *Phys. Rev. A* **81**, 052105 (2010).
- [63] R. Schmidt, A. Negretti, J. Ankerhold, T. Calarco, and J. T. Stockburger, *Phys. Rev. Lett.* **107**, 130404 (2011).
- [64] R. Blatt, P. Zoller, G. Holz Müller, and I. Siemers, *Zeitschrift für Phys. D Atoms, Mol. Clust.* **4**, 121 (1986).
- [65] C. Zerbe, P. Jung, and P. Hänggi, *Phys. Rev. E* **49**, 3626 (1994).
- [66] S. Arnold, J. H. Li, S. Holler, A. Korn, and A. F. Izmailov, *J. Appl. Phys.* **78**, 3566 (1995).
- [67] J. T. Stockburger and H. Grabert, *Phys. Rev. Lett.* **88**, 170407 (2002).
- [68] R. Schmidt, S. Rohrer, J. Ankerhold, and J. T. Stockburger, *Phys. Scr.* **T151**, 014034 (2012).
- [69] S. Rahimi-Keshari, T. Kiesel, W. Vogel, S. Grandi, A. Zavatta, and M. Bellini, *Phys. Rev. Lett.* **110**, 160401 (2013).
- [70] K. K. Sabapathy, *Phys. Rev. A* **93**, 042103 (2016).
- [71] H.-B. Chen, C. Gneiting, P.-Y. Lo, Y.-N. Chen, and F. Nori, *Phys. Rev. Lett.* **120**, 030403 (2018).
- [72] Arvind, N. Mukunda, and R. Simon, *Phys. Rev. A* **56**, 5042 (1997).
- [73] H. R. Lewis and W. B. Riesenfeld, *J. Math. Phys.* **10**, 1458 (1969).
- [74] K. F. Riley, M. P. Hobson, and S. J. Bence, *Mathematical Methods for Physics and Engineering*, 3rd ed. (Cambridge University Press, 2006) p. 1359.